Received: 19 July 2016 | Accepted: 22 March 2017

DOI: 10.1111/faf.12225

ORIGINAL ARTICLE

WILEY FISH and FISHERIES

The relative influence of temperature and size-structure on fish distribution shifts: A case-study on Walleye pollock in the Bering Sea

James T Thorson[1] | James N Ianelli[2] | Stan Kotwicki[2]

[1]Fisheries Resource Assessment and Monitoring Division, Northwest Fisheries Science Center, National Marine Fisheries Service, NOAA, Seattle, WA, USA

[2]Resource Ecology and Fisheries Management Division, Alaska Fisheries Science Center, National Marine Fisheries Service, NOAA, Seattle, WA, USA

Correspondence
James T Thorson, Fisheries Resource Assessment and Monitoring Division, Northwest Fisheries Science Center, National Marine Fisheries Service, NOAA, Seattle, WA, USA.
Email: james.thorson@noaa.gov

Abstract

Research has estimated associations between water temperature and the spatial distribution of marine fishes based upon correlations between temperature and the centroid of fish distribution (centre of gravity, COG). Analysts have then projected future water temperatures to forecast shifts in COG, but often neglected to demonstrate that temperature explains a substantial portion of historical distribution shifts. We argue that estimating the proportion of observed distributional shifts that can be attributed to temperature vs. other factors is a critical first step in forecasting future changes. We illustrate this approach using *Gadus chalcogrammus* (Walleye pollock) in the Eastern Bering Sea, and use a vector-autoregressive spatiotemporal model to attribute variation in COG from 1982 to 2015 to three factors: local or regional changes in surface and bottom temperature ("temperature effects"), fluctuations in size-structure that cause COG to be skewed towards juvenile or adult habitats ("size-structured effects") or otherwise unexplained spatiotemporal variation in distribution ("unexplained effects"). We find that the majority of variation in COG (including the north-west trend since 1982) is largely unexplained by temperature or size-structured effects. Temperature alone generates a small portion of primarily north–south variation in COG, while size-structured effects generate a small portion of east–west variation. We therefore conclude that projections of future distribution based on temperature alone are likely to miss a substantial portion of both the interannual variation and interdecadal trends in COG for this species. More generally, we suggest that decomposing variation in COG into multiple causal factors is a vital first step for projecting likely impacts of temperature change.

KEYWORDS

Alaska pollock, distribution shift, size-structure, spatiotemporal model, temperature impacts

1 | INTRODUCTION

The Walleye pollock (*Gadus chalcogrammus*, Gadidae; hereafter referred to as pollock) stock in the Bering Sea supports an industry worth over $1 billion annually (in first sale wholesale prices; Fissel et al., 2015) and is the focus of extensive data collection and research. Previous authors (Kotwicki, Buckley, Honkalehto, & Walters, 2005; Wyllie-Echeverria & Wooster, 1998) have shown that the spatial distribution of pollock varies between "warm" and "cool" years in the Eastern Bering Sea, where warm years commence with winter sea-ice having a maximum extent that is skewed north relative to long-term averages and cool years have a southward-skewed distribution for winter sea-ice. Maximum sea-ice extent is strongly associated with the proportion of the Bering Sea with low bottom temperatures (the

area of the "cold pool"; Stabeno, Bond, Kachel, Salo, and Schumacher, 2001), and the cold pool has been shown to affect the distribution of demersal fishes such as pollock (Kotwicki & Lauth, 2013). Previous analyses have generally studied the impact of temperature or cold pool area in isolation, without attempting to estimate what proportion of variance in pollock distribution is explained by temperature relative to other factors.

Ecological studies often seek to estimate a link between temperature and distribution, and then use this linkage to forecast shifts in distribution given changing global temperatures due to long-term climate shifts. Examples include Perry, Low, Ellis, and Reynolds (2005), which regressed a sample-based calculation for centre of gravity (COG) for North Sea fishes against a moving average of bottom temperature, and concluded that bottom temperature and northward COG were related. Similarly, Cheung et al. (2009) fitted a climate envelope model using temperature as an explanatory variable to distribution for many marine species, and then projected likely changes in climate envelopes given different scenarios for future temperature. However, neither study quantifies the proportion of variation in distribution that is explained by temperature. By contrast, we argue that studies of spatial distribution and dynamics should include two features: (i) an analysis demonstrating a link between a causal variable (e.g., temperature) and a population variable (centre of distribution); and (ii) an attempt to quantify predictive uncertainty for the forecast. In particular, when a variable explains a small portion of total variance in distribution, forecasts will likely explain a correspondingly small portion of future variability.

In addition to temperature, the spatial distribution of fish populations may be affected by ontogenetic shifts as individuals age and grow (e.g., Gratwicke, Petrovic, & Speight, 2006; Hicks, Taylor, Grandin, Taylor, & Cox, 2014). Diet data from pollock have shown cannibalism which has led to hypotheses on possible evolutionary incentives for juveniles to minimize cannibalism by occupying different habitat than adults (Bailey, 1989). Given that juveniles and adults tend to have different spatial distributions, recruitment variation alone can affect the spatial distribution of pollock (e.g., where years following strong recruitment will be skewed towards the juvenile habitats). In the following, we term this mechanism a "size-structured effect". This affects distribution shifts whenever (i) juveniles and adults have strong spatial differences in distribution; (ii) recruitment variation is high; and (iii) generation time is low, due to high natural and/or fishing mortality rates. Conditions (ii) and (iii) both contribute to high variation in size-structure over time.

The spatial distribution of fishes may change following many other density-dependent and density-independent processes in addition temperature and size-structured effects. Previous studies report variability among years in timing of spawning and feeding migrations (e.g., Ernst, Orensanz, & Armstrong, 2005; Kotwicki et al., 2005; Nichol, 1998), in situ light conditions driving changes in distribution within feeding habitats (Kotwicki, De Robertis, von Szalay, & Towler, 2009), primary production patterns and fishing pressure (Garrison et al., 2010). Distribution may also change due to density-dependent expansion of the population's range (Kotwicki & Lauth, 2013; Spencer, 2008), changes in food availability (e.g., Dorn, 1995; Nøttestad, Giske, Holst, & Huse, 1999) and interactions with other species including competition and predation (Ciannelli, Fauchald, Chan, Agostini, & Dingsør, 2008).

In this study, we develop a method to quantify the contribution of temperature, size-structure and other factors that contribute to shifts in the spatial distribution of marine fishes. This method specifically decomposes variation in catch rates into components caused by changes in distribution (encounter/non-encounter) and density (catch rates given that the species is encountered) to distinguish between these two mechanisms for changing distribution. We demonstrate this method using pollock as a case-study example, and seek to answer: (i) Can changes in temperature or size-structure generate substantial variation in COG over time for this species; and (ii) do the shifts caused by temperature or size-structure explain observed patterns in COG for pollock?

2 | METHODS

2.1 | Overview

We seek to model changes over time in the spatial distribution of different size-categories for marine fishes. We chose to use a delta-model, which separately estimates the probability p that a given sample will encounter the species, and the expected catch rate r given that the species is encountered (Maunder & Punt, 2004). Specifically, sampled biomass b_i (in kg) for each sample i is modelled as:

$$\Pr(b_i = B) = \begin{cases} 1 - p_i & \text{if } B = 0 \\ p_i \times \text{Gamma}(B|\theta_c^{-2}, a_i r_i \theta_c^2) & \text{if } B > 0 \end{cases},$$

where r_i is the catch rate (in kg/km^2) for sample i, $\text{Gamma}(B|\theta_c^{-2}, a_i r_i \theta^2)$ is the gamma probability density function evaluated at B given shape θ^{-2} and scale $r_i\theta_c^2$, and θ_c is the coefficient of variation for positive catches for size-class c. We use this delta-gamma function so that we can separately interpret predictors of spatial variation in encounter probability and positive catch rates. Given estimates of encounter probability and positive catch rate, we can then predict population density (in kg/km^2) at each sampled location as $d_i = p_i \times r_i$.

We use a vector-autoregressive spatiotemporal (VAST) model to decompose sampling variation into different biologically interpretable sources (Thorson & Barnett, 2017). We include three distinct sources of variation in both encounter probability and expected catch rates:

1. *Intercepts*—We incorporate annual variation in average encounter probability, p, and positive catch rates, r, across locations within the spatial domain of the model. This annual variation represents changes among years in the proportion of population abundance belonging to different size-classes.
2. *Covariates*—We incorporate measured habitat variables as predictors of p and r, which allows us to estimate the impact of measureable covariates on local density. Specifically, we incorporate responses to both local and regional variation in temperature.

3. *Residual spatial and spatiotemporal variation*—We account for two sources of residual variation in p and r for each size-class. The first source involves estimating spatial autocorrelation terms for each size-class. These estimates are constant over time, and thus can be considered as representing unmeasured habitat variables that do not change over the modelled period (e.g., depth, sediment size). The second set of terms is to account for autocorrelation in p and r that changes among years and spatial locations. This latter spatiotemporal variation represents the influence of unmeasured habitat variables that change among years, and accounts for shifts in distribution for each size-class beyond the shifts predicted by covariates (e.g., temperature).

We interpret this as a "semi-parametric" model because it includes annually varying intercepts, measured covariates and residual spatial and spatiotemporal variation (Shelton, Thorson, Ward, & Feist, 2014). We use mixed-effects methods for parameter estimation, and this approach identifies parameters that minimize residual spatial and spatiotemporal variation by maximizing the variation attributed to intercepts and covariates (items 1 and 2 above). We note that the model has some similarities to classical universal Kriging (Petitgas, 2001), but allows additional flexibility regarding the distribution of measurement errors and the covariance among size-classes.

2.2 | Vector-autoregressive spatiotemporal model

Encounter probability p_i and expected catch rates r_i for each sample i are affected by the predicted density of individuals or groups λ_i (in numbers/km^2) at the time t_i, location s_i, and length-bin c_i associated with that sample:

$$\log(\lambda_i) = \gamma_\lambda(t_i, c_i) + \omega_\lambda(s_i, c_i) + \varepsilon_\lambda(s_i, c_i, t_i) + \sum_{k=1}^{n_k} \alpha_{k,c_i} x_k(s_i, c_i, t_i),$$

where $\gamma_\lambda(t_i, c_i)$ is an intercept that governs the expectation across space of numbers-density for a given time and length-bin, $\alpha_{k,c}$ is a coefficient that governs the effect of a covariate $x_k(s_i, c_i, t_i)$ on numbers-density associated with a given location, bin and time, $\omega_\lambda(s_i, c_i)$ represent spatial variation in numbers-density λ_i, and $\varepsilon_\lambda(s_i,c_i,t_i)$ represents spatiotemporal variation. We use a log-link to ensure that predicted numbers-density λ_i is positive.

The probability of encounter p_i for sample i is derived from a Poisson process, given a random distribution of λ_i groups of individuals in the vicinity of a given location and time:

$$p_i = 1 - \exp(-a_i \times \lambda_i),$$

where a_i is the area sampled (in units of square kilometres) by the i-th sample (i.e., a complementary log-log-link for p_i). The expected catch rate r_i given that a sample encounters a given species then depends upon expected numbers-density and average weight w_i for each group of individuals:

$$\log(w_i) = \gamma_w(t_i, c_i) + \omega_w(s_i, c_i) + \varepsilon_w(s_i, c_i, t_i) + \sum_{k=1}^{n_k} \beta_{k,c_i} x_k(s_i, c_i, t_i),$$

where parameters are defined identically to those for numbers-density except that we use subscripts λ and w to distinguish between parameters for the two components. Specifically, expected catch rate given an encounter is calculated as:

$$r_i = \frac{\lambda_i}{p_i} \times w_i,$$

where the model is parameterized such that predicted biomass density $d = \lambda \times w = p \times r$. This model for numbers-densities λ_i and average weight w_i has a similar number of parameters to a conventional delta-generalized linear mixed model, although it offers the benefit of specifying covariates via a log-link for both components (rather than a logit-link for encounter probability in a conventional delta-model) and covariate effects are therefore more easily interpretable.

Residual spatial variation is treated as a three-dimensional Gaussian process (termed a "Gaussian random field"), with correlations over two spatial dimensions (e.g., eastings and northings) and among length-bins:

$$\mathrm{vec}(\boldsymbol{\Omega}_\lambda) \sim \mathrm{GRF}(0, \mathbf{R}_\lambda \otimes \mathbf{V}_{\omega\lambda}),$$

where $\boldsymbol{\Omega}_\lambda$ is a matrix composed of $\omega_\lambda(s_i, c_i)$ at every location s and length-bin c, $\mathbf{R}_\lambda$ is the correlation among locations, and $\mathbf{V}_{\omega\lambda}$ is the covariance among length-bins for spatial variation in population density (where $\boldsymbol{\Omega}_w$ is defined identically but with $\mathbf{R}_w$ and $\mathbf{V}_{\omega w}$ in place of $\mathbf{R}_w$ and $\mathbf{V}_{\omega w}$). Spatial correlation $\mathbf{R}_\lambda$ for encounter probabilities follows a Matérn process:

$$\mathbf{R}_\lambda(s, s^*) = \frac{1}{2^{\nu-1}\Gamma(\nu)} (\kappa_\lambda \mathbf{H}|s - s^*|)^\nu K_\nu(\kappa_\lambda \mathbf{H}|s - s^*|),$$

where ν is smoothness (fixed at 1.0), κ_λ governs the distance over which locations are uncorrelated (and where $\mathbf{R}_r$ is defined identically but with κ_r in place of κ_λ), K_ν is a Bessel function, and $\mathbf{H}$ is a two-dimensional linear transformation representing geometric anisotropy (i.e., the tendency for correlations to decrease more slowly with distance along one axis than another, see Bez (2002: fig. 3) or Thorson, Shelton, Ward, and Skaug (2015)). Covariance $\mathbf{V}_{\omega\lambda}$ among length-bins for $\boldsymbol{\Omega}_\lambda$ (the random effect representing spatial variation in encounter probabilities) is approximated using a factor decomposition:

$$\mathbf{V}_{\omega\lambda} = \mathbf{L}_{\omega\lambda} \mathbf{L}_{\omega\lambda}^{\mathsf{T}},$$

where $\mathbf{L}_{\omega\lambda}$ is a n_c by n_f matrix where $0 \le n_f \le n_c$ is the rank of $\mathbf{V}_{\omega\lambda}$ such that $\mathbf{V}_{\omega\lambda}$ is a reduced-rank approximation to covariance among bins (Thorson, Scheuerell, et al., 2015; Warton et al., 2015), and $\mathbf{V}_{\omega r}$ is defined identically but with $\mathbf{L}_{\omega r}$ in place of $\mathbf{L}_{\omega\lambda}$. Similarly, spatiotemporal variation in each year is treated as a three-dimensional Gaussian process, following a Matérn process over space and a first-order autoregressive process over length-bins:

$$\mathrm{vec}(\boldsymbol{\varepsilon}_\lambda(t)) \sim \mathrm{GRF}(0, \mathbf{R}_\lambda \otimes \mathbf{V}_{\varepsilon\lambda}),$$

where $\boldsymbol{\varepsilon}_r(t)$ is defined identically but with $\mathbf{R}_r$ and $\mathbf{V}_{\varepsilon r}$ in place of $\mathbf{R}_\lambda$ and $\mathbf{V}_{\varepsilon\lambda}$. We specify a different covariance among length-bins for spatial ($\mathbf{V}_{\omega\lambda}$) and spatiotemporal ($\mathbf{V}_{\varepsilon\lambda}$) variation.

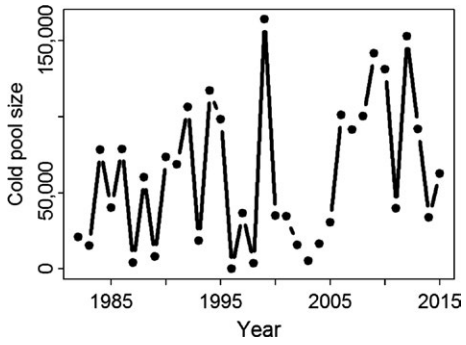

FIGURE 1 Cold pool size (in units of square kilometres) during the modelled period, where the interaction of cold pool size and both eastings and northings is included as a "regional" temperature variable in our model

Previous analyses of distribution shifts have emphasized temperature as an important driver (Pinsky, Worm, Fogarty, Sarmiento, & Levin, 2013), so we include both the effect of temperature at the location and time of the survey ("local temperature") and the effect of changes in average temperature throughout the Eastern Bering Sea in a given year ("regional temperature"). We model a local temperature effect by including a quadratic relationship between local temperature and both encounter probability and positive catch rates (Fig. S1). We also include the regional temperature effect by including the interaction of eastings (or northings) with the area of the cold pool (Figure 1). Hypothetically, if a large cold pool is associated with a southward shift in distribution, then this would result in a significant estimate of the coefficient linking the northings-cold pool variable to either λ or $\boldsymbol{w}$. In summary, we include four covariates:

$$\mathbf{x}(s,c,t) = (T(s,t), T^2(s,t), N(s)A(t), E(s)A(t))^{\mathsf{T}},$$

where $T(s, t)$ is the bottom temperature associated with location $\boldsymbol{s}$ and year t, $T^2(s, t)$ is bottom temperature-squared (i.e., we include a quadratic effect of bottom temperature), $N(s)$ and $E(s)$ are northings and eastings for location s, and $A(t)$ is an annual index of cold pool area (defined as the area in kilometres-squared for bottom temperatures of 0°C or colder) for year t. Inspection of bottom temperatures shows that the cold pool was relatively large in 1999, and 2003–2004 and 2006, and essentially absent in 1987, 1996, 1998 and 2003 (Figure 1 and Fig. S1).

We estimate parameters for this VAST model by maximizing the marginal likelihood of parameters given available data (see Table 1 for a list of fixed and random effects). Fixed effects include intercepts for each year and size-category for numbers-density and average weight ($\gamma_\lambda(c, t)$ and $\gamma_w(c, t)$), the spatial scale for spatial correlations (κ_λ and κ_w) and geometric anisotropy ($\mathbf{H}$), the covariance among length-bins for spatial ($\mathbf{L}_{\omega\lambda}$ and $\mathbf{L}_{\omega w}$) and spatiotemporal ($\mathbf{L}_{\varepsilon\lambda}$ and $\mathbf{L}_{\varepsilon w}$) variation, measurement parameters (θ_c for each size-class $\boldsymbol{c}$) and the effect of measured covariates ($\alpha_{k,c}$ and $\beta_{k,c}$). Mixed-effect estimation will generally favour a solution that minimizes residual variation (i.e., a simultaneously low value for variance θ_c, $\mathbf{L}_{\omega\lambda}$, $\mathbf{L}_{\omega w}$, $\mathbf{L}_{\varepsilon\lambda}$ and $\mathbf{L}_{\varepsilon w}$), and it does so by first attributing variation to fixed effects (intercepts and covariates) and only then attributing model residuals to spatial and spatiotemporal variation. We treat spatial variation ($\boldsymbol{\Omega}_\lambda$ and $\boldsymbol{\Omega}_r$) and spatiotemporal variation ($\mathbf{E}_\lambda$ and $\mathbf{E}_r$) as random effects, and approximate the marginal likelihood across these random effects using the Laplace approximation (Skaug & Fournier, 2006). Parameter estimation is conducted using Template Model Builder (Kristensen, Nielsen,

TABLE 1 A list of parameters and symbols defined in the main text

Name	Symbol
Notation for explaining theory	
Predicted population density	d
Expected numbers-density	λ
Expected average weight	w
Expected encounter probability	p
Expected positive catch rates	r
Indices	
Observation	i
Covariate	k
Year	t
Length-bin	c
Location	j
Overdispersion factor	f
Dimensionality	
Number of observations	n_i
Number of covariates	n_k
Number of years	n_t
Number of length-bins	n_c
Number of locations	n_j
Number of factors for overdispersion	n_f
Data	
Catch rate for observation i	b_i
Location for observation i	s_i
Length-bin for observation i	c_i
Year for observation i	t_i
Measured covariates for observation i	$\mathbf{x}(s_i, c_i, t_i)$
Parameters (fixed effects)	
Intercept for λ_i	$\gamma_\lambda(t, c)$
Covariate effects for λ_i	$\alpha_{k,c}$
Covariate effects for w_i	$\beta_{k,c}$
Pointwise variance in spatial variation in λ_i	$\sigma^2_{\lambda,\omega}$
Decorrelation distance for spatial and spatiotemporal variation in λ_i	κ_λ
Covariation among bins in spatial and spatiotemporal variation in λ_i	$\mathbf{L}_\lambda$
Rotation matrix representing geometric anisotropy	$\mathbf{H}$
Pointwise variance in spatiotemporal variation in λ_i	$\sigma^2_{\lambda,\xi}$
Random effects	
Spatial variation in λ_i	$\omega_\lambda(s, c)$
Spatiotemporal variation in λ_i	$\varepsilon_\lambda(s, c, t)$

Berg, Skaug, & Bell, 2016) in the R statistical environment (R Core Team, 2015). We use the stochastic partial differential equation approximation to the probability of random effects (Lindgren, Rue, & Lindström, 2011), and also use a "predictive process" approximation wherein spatial and spatiotemporal components are approximated as being piecewise constant at 100 locations (termed "knots") that are selected using a k-means algorithm applied to the location of sampling data. R package VAST for implementing this model for other data sets is publicly available on the first author's GitHub site (https://github.com/James-Thorson/VAST).

2.3 | Case-study: Alaska pollock

As case-study, we analyse catch rate data for pollock from the Eastern Bering Sea (EBS). Specifically, we use data collected during standardized EBS bottom trawl surveys conducted by the Alaska Fisheries Science Center since 1982 (Stauffer, 2004). Annual surveys were conducted in June and July over the fixed set of approximately 376 stations and used the same standard trawl (83–112 eastern otter trawl) during all years. Surveys started in the south-eastern corner of the survey area and proceeded westward. Tow duration was approximately 30 min at 1.54 m/s (3 knots). A subsample of 150–200 individuals from each tow were measured to the nearest centimetre using fork length, and this subsample was then expanded to represent the entire tow catch (using the ratio of sampled weight and tow weight for that species). The catch rate in number per hectare was estimated using the area-swept method (e.g., Alverson and Pereyra, 1969) by multiplying distance fished, as indicated by bottom contact sensor (Somerton & Weinberg, 2001), by the average distance between wing tips measured using acoustic spread sensors (see Weinberg and Kotwicki (2008) for details). We analysed catch rate data for five size-categories: 0–20 cm (mostly age-1 individuals), 21–30 cm (mostly age-2 individuals), 31–40 cm, 41–50 cm and 50+ cm individuals. Given the relatively small number of size-categories, we used full rank for all covariance matrices (i.e., $n_f = 5$, such that $\mathbf{V}_{\omega\lambda}$, $\mathbf{V}_{\varepsilon\lambda}$, $\mathbf{V}_{\omega r}$ and $\mathbf{V}_{\varepsilon r}$ each involve estimating 15 unique parameters).

Prior to analysis, we converted catch rate for each length category from numbers to weight (kilograms), using a year-specific length–weight relationship obtained for years when length–weight samples were collected (i.e., 1991, and 1999–2016). For remaining years, the average length–weight relationship was obtained by pooling all available data. We also corrected catch rate estimates for density-dependent sampling efficiency of the survey bottom trawl (Kotwicki, Ianelli, & Punt, 2014). We analyse data from 1982 to 2015, where this period includes a marked decrease and recovery of pollock abundance in the EBS between 2008 and 2015 (Ianelli, Honkalehto, Barbeaux, & Kotwicki, 2015).

2.4 | Calculating centre of gravity

We summarize shifts in distribution by calculating the centroid of the distribution for a given size-category and year (termed centre of gravity, COG). To do so, we first calculate the biomass density $d(s, c, t)$ for size-class c associated with every location and year:

$$\begin{aligned} d(s,c,t) &= a(s)\times\lambda(s,c,t)\times w(s,c,t) \\ &= a(s)\times\exp\left(\gamma_\lambda(t,c)+\omega_\lambda(s,c)+\varepsilon_\lambda(s,c,t)+\sum_{k=1}^{n_k}\alpha_{k,c_i}x_k(s,c,t)\right), \\ &\times\exp\left(\gamma_w(t,c)+\omega_w(s,c)+\varepsilon_w(s,c,t)+\sum_{k=1}^{n_k}\beta_{k,c_i}x_k(s,c,t)\right) \end{aligned}$$

where $a(s)$ is the area associated with modelled location s. We then calculate a model-based estimate of the COG from predicted density throughout the population domain:

$$\bar{x}(c,t)=\frac{\sum_{s=1}^{n_s}d(s,c,t)x(s)}{\sum_{s=1}^{n_s}d(s,c,t)},$$

where $x(s)$ is a suitable description of location for site s. This formula for COG standardizes by total abundance (in the denominator), so our analysis focuses on changes in distribution after controlling for changes in total abundance. Future research could alternatively explore temperature impacts on total abundance and/or density-dependent impacts on COG. In the following, we use either eastings/northings in kilometres (when calculating summaries of distance, where eastings and northings are calculated using a projection that has minimal distortion of distance), or latitude/longitude in degrees (when plotting results on a map). Previous research suggests that model-based estimates of COG are in some cases more statistically efficient than conventional sample-based estimators (Thorson, Pinsky, & Ward, 2016).

2.5 | Counterfactual model exploration

We distinguish the following three hypotheses for explaining changes in distribution over time: (i) temperature; (ii) size-structure; and (iii) residual variation. These hypotheses are not mutually exclusive, so we seek to estimate what proportion of variance in COG is explained by each of these factors. To do so, we take estimated values of fixed and random effects for the fitted model, and fix some subset to zero to exclude individual processes from the model. For each "counterfactual run," we then recalculate the time series of northward and eastward COG that would result from that subset of parameters. Specifically:

1. *Temperature*—To isolate the effect of temperature, we eliminate any variation in size-structure (i.e., fix intercepts for average numbers-density and average weight for a given size-class and year at its average over all years) and eliminate residual spatiotemporal variation, but leave temperature effects at their estimated value. We then use these values to predict biomass density $d = \lambda \times r$ for all sites, and calculate COG using these values.
2. *Size-structure*—To isolate the effect of variation in size-structure, we eliminate temperature effects and residual spatiotemporal variation. We leave interannual variation in the proportion of total

TABLE 2 Hypothesized drivers of distribution shift, a verbal description of how these potentially impact distribution for Alaska pollock, how these mechanisms are represented in the vector-autoregressive spatiotemporal model, and how the relative importance of these hypothesized drivers is assessed using the parameters estimated for Alaska pollock

Hypothesized driver	Description of mechanism	Description of test for relative importance of mechanism	Quantitative test for hypothesis
Temperature	Variation in temperature drives changes in distribution among years, either via: 1. Localized response of density to local temperature; or 2. Change in spatial distribution of population due to regional temperature	Eliminate alternative mechanisms for distribution shift, that is: 1. Changes in the proportion of the population belonging to different size-classes; and 2. Residual spatiotemporal variation in density after controlling for temperature and size-structured variation.	Eliminate variation caused by alternative mechanisms, that is: 1. Fixing intercepts (representing variation among years in the proportion of the population belonging to different size-classes) at their average values across years, $\gamma_\lambda(c,t) = n_t^{-1}\sum_{t=1}^{n_t}\gamma_\lambda(c,t)$ and $\gamma_w(c,t) = n_t^{-1}\sum_{t=1}^{n_t}\gamma_w(c,t)$; and 2. Fixing residual spatiotemporal variation at zero, $\varepsilon_\lambda(s,c,t) = 0$ and $\varepsilon_w(s,c,t) = 0$
Size-structure	Variation in cohort strength, when combined with differences in the spatial distribution for different size-classes, results in a population distribution skewed towards the distribution for the dominant size-class in a given year.	Eliminate alternative mechanisms, that is: 1. Local or regional impacts of temperature on density; and 2. Residual spatiotemporal variation in density after controlling for temperature and size-structured variation.	Eliminate variation caused by alternative mechanisms, that is: 1. Fixing the impact of covariates at zero, $\alpha(s,c) = 0$ and $\beta(s,c) = 0$; and 2. Fixing residual spatiotemporal variation at zero, $\varepsilon_\lambda(s,c,t) = 0$ and $\varepsilon_w(s,c,t) = 0$
Unexplained variation	Otherwise unmodelled processes (e.g., shifts in the spatial distribution of predators or resources, interannual variation in where cohorts settle and mature) drive changes in distribution among years.	Eliminate alternative mechanisms, that is: 1. Changes in the proportion of the population belonging to different size-classes; and 2. Local or regional impacts of temperature on density	Eliminate variation caused by alternative mechanisms, by: 1. Fixing intercepts (representing variation among years in the proportion of the population belonging to different size-classes) at their average values across years, $\gamma_\lambda(c,t) = n_t^{-1}\sum_{t=1}^{n_t}\gamma_\lambda(c,t)$ and $\gamma_w(c,t) = n_t^{-1}\sum_{t=1}^{n_t}\gamma_w(c,t)$; and 2. Fixing the impact of covariates at zero, $\alpha(s,c) = 0$ and $\beta(s,c) = 0$

abundance belonging to different size-classes and again calculate COG using these values.

3. *Unexplained variation*—To isolate the portion of variation that is not explained by size-structure or temperature, we eliminate variation in size-structure and fix temperature effects at zero, and again calculate COG using these values.

Further details about how we implement these counterfactual models are provided in Table 2. In an exploratory run, we also confirm that eliminating variation in cohort strength, and fixing both temperature and unexplained variation at zero results in no variance in COG. This confirms that all estimated variation in COG is attributable to one of these three processes.

3 | RESULTS

We first visualize northward and eastward COG for each of five size-categories (Figure 2). This shows that individuals with size 21–30 and 31–40 cm have a COG to the northwest, and individuals with size 50+ have a COG to the south-east of the average COG for the entire population. The proportion of total biomass represented by individuals of size 0–40 cm has decreased over time (particularly during the early 1980s), while the proportion with size 50 cm or greater has increased (particularly prior to 1995). We therefore conclude that variation in size-structure has caused a southward shift in distribution over time towards the COG for large individuals, with the greatest shift caused by size-structure occurring from 1982 to 1990.

Next, we show density maps for total biomass, as well as the three counterfactual scenarios generated by excluding all mechanisms for variation in COG except temperature, recruitment variation or otherwise unexplained variation (Figure 3). Relative to other years, density is high near the Alaskan peninsula in 1995, and is relatively high in the north-western portion in 2008 and 2015 (Figure 3, 1st column). The counterfactual scenario restricting variation to temperature effects (Figure 3, 2nd column) shows that temperature in isolation explains relatively little variation in density among years, although it contributes to the elevated density in the southern boundary in 1995 and 2008. By contrast, changes in size-structure in isolation (Figure 3, 3rd column) can generate the relatively high-density inshore in 2008 relative to 1982 and 1989. Nevertheless, general patterns in spatiotemporal variation are mainly unexplained (Figure 3, 4th column); for example, the relative increase in densities in the northern portion of the populations range in 2008 and 2015 is attributed primarily to unexplained variation.

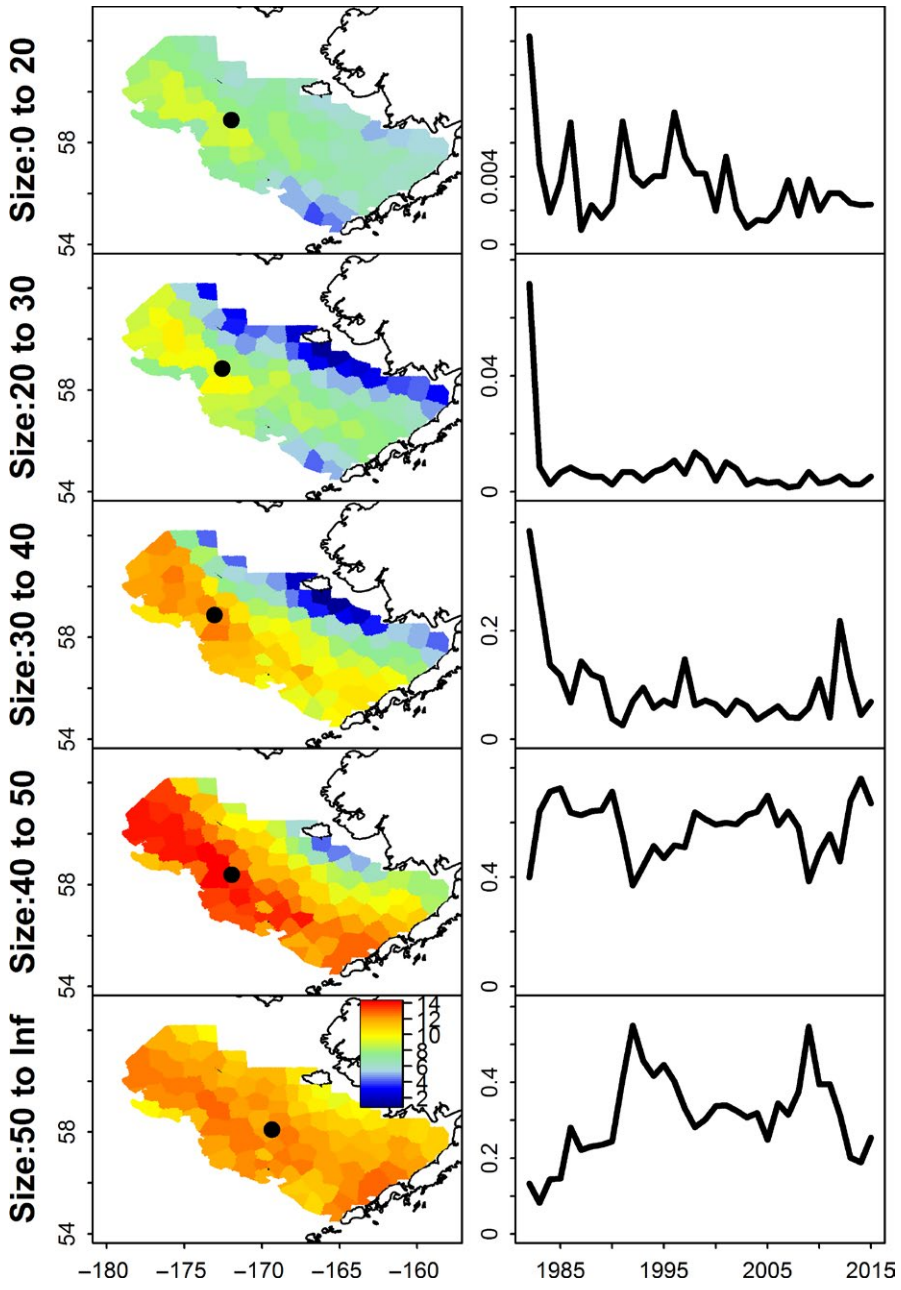

FIGURE 2 Estimated log-density for pollock (colour legend is provided in the bottom row and has units ln(kg/km^2)) on average across years of five different sizes classes (1st column, where centre of gravity for each size-class is shown as a black point), and proportion of biomass for that size-class in each year (2nd column, where the *y*-axis range varies for each size-class)

Next, we compute the standard deviation of COG for each counterfactual scenario (Table 3). This shows the strong agreement between our model-based estimates of COG and a simple abundance-weighted average estimator, where both show a standard deviation of approximately 70–75 km east–west and 45–50 km north–south. Temperature in isolation accounts for more northward (21 km) than eastward (13 km) variation, while variation in size-structure accounts for greater variation east–west (23 km) than north–south (7 km). The greatest standard deviation by far is attributed to "unexplained variation" in density.

Finally, inspection of COG estimates for each counterfactual scenario clearly confirms that observed variation in COG is primarily attributable to unexplained variation (Figure 4). As expected, size-structure causes a southward and eastward trend in COG from 1982 to nearly 2010, and causes greater variation east–west than north–south. By contrast, temperature generates strong interannual variation along the north–south axis. However, the estimated COG moved nearly 100 km north and west from 1982 to 2015, and neither temperature nor size-structure captures this trend. Similarly, observed COG exhibits high interannual variation (e.g., a large shift northward from 1994 to 1997 and westward from 2003 to 2006), and neither temperature nor size-structure explains this interannual variation.

4 | DISCUSSION

In this study, we have developed a statistical approach for decomposing variation in species distribution into components attributable to local and regional temperature, variation in size-structure

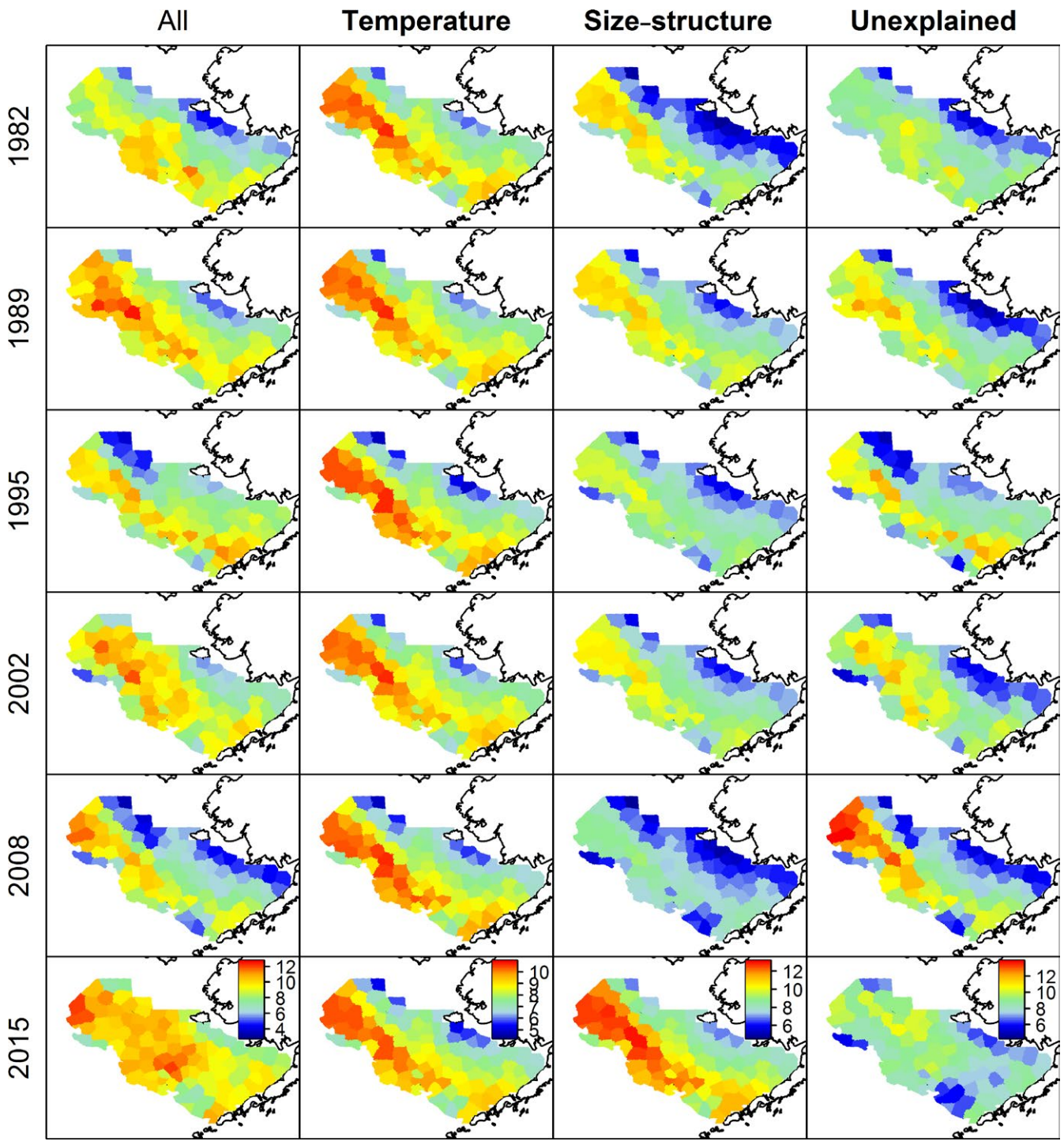

FIGURE 3 Estimated log-density for pollock (1st column) compared with counterfactual scenarios that eliminate all causes for variation in distribution except temperature (2nd column), recruitment variation (3rd column) or unexplained variation (4th column), for six evenly spaced years (rows) (colour scale differs among columns; colour legend is provided in the bottom row and has units ln(kg/km^2))

and otherwise unexplained variation in density. We demonstrated this approach using the extensive and consistent data collections for pollock, one of the most valuable fisheries in the USA. Results showed that temperature and size-structure by themselves generate a smaller variance in COG than is observed and that shifts in distribution predicted by temperature and size-structure do not capture long-term shifts to the north-west for this species. This result is surprising, given the many studies that have previously attributed range shifts for this species to temperature affects (e.g., Kotwicki et al., 2005; Wyllie-Echeverria & Wooster, 1998). However, this difference likely arises because previous studies have generally not attempted to quantify what portion of variation in distribution is attributable to

TABLE 3 Standard deviation of variation in centre of gravity (COG) among years in eastings and northings (in units of kilometres). We show the variation observed in the pollock bottom trawl data (using a model-free "abundance-weighted average" estimator), compared with the variation associated with hypothesized drivers of distribution shift (temperature, cohort effects or residual variation)

	Northings COG (km)	Eastings COG (km)
Abundance-weighted average estimator	44.6	70.4
Full model	50.7	72.2
Only temperature	19.7	11.3
Only size-structure	12.1	35.5
Only unexplained	60.4	89.1

temperature, and have therefore failed to recognize that previously identified effects of temperature explain a small portion of interannual or decadal variation. However, we note that Kotwicki and Lauth (2013) had similarly concluded that the trend towards the north-west in pollock is not directly related to changes in temperatures, and had hypothesized that fishing in the southern portion might be an alternative hypothesis. We therefore recommend future research to integrate spatial information regarding fishing effort into a VAST model (perhaps by using lagged fishing effort as a covariate) to explore whether the "unexplained variation" from this study can be attributed to human harvest.

More generally, we argue that any study regarding the likely impacts of future environmental changes (e.g., changes in sea-ice cover or bottom temperatures) should first quantify the proportion of historical variation that can be explained by the variables that are available for forecasting. Given that the trend towards the north-west for pollock is not explained by historical temperature effects, the likely impact of future temperature changes may also be swamped by otherwise unexplained factors affecting distribution for this species. Accurately quantifying uncertainty is increasingly recognized as vital to the use and credibility of any scientific model (Silver, 2015), and we similarly believe that it is vital for making credible predictions of climate impacts on marine fishes.

We acknowledge that it is unsettling that two dominant hypotheses (temperature and size-structure) explain a relatively small portion of variation in COG for pollock, and we advocate for future research to decompose "unexplained variation" into different biological mechanisms. One avenue for research involves identifying patterns in distribution shifts for multiple species simultaneously, and cataloguing the physical or ecological variables that could simultaneously explain distributions shifts for multiple species. Spatiotemporal variation in density for pollock is strongly correlated with Pacific cod (*Gadus macrocephalus*, Gadidae; Thorson, Ianelli, et al. (2016)), and this suggests that there are shared environmental factors driving productivity for these phylogenetically related species. Productivity for pollock is likely impacted by species interactions (Spencer et al., 2016), so we recommend ongoing research regarding species interactions (competition and predation) in spatiotemporal statistical models. For example, interactions with the expanding spatial distribution of arrowtooth flounder could potential explain distribution shifts for juvenile pollock, either due to behavioural avoidance or direct predation (Spencer et al., 2016), and these competitive or predator/prey impacts could be integrated if species interactions were explicitly modelled (e.g., Thorson, Munch, & Swain, 2017).

Another potential mechanism that is missing in our model is the settlement of individual cohorts within particular spatial areas, which could cause COG to vary as it tracks spatial patterns in settlement of dominant cohorts over time. This process could presumably be modelled by explicitly modelling the settlement and growth of individual cohorts (Kristensen, Thygesen, Andersen, & Beyer, 2014; Thorson, Ianelli, Munch, Ono, & Spencer, 2015). However, integrating this hypothesis with habitat partitioning by different size-classes would presumably require an explicit spatiotemporal model for individual movement rates by size-class. Although spatiotemporal analysis of individual movement is feasible using advective-diffusive modelling techniques (Sibert, Hampton, Fournier, & Bills, 1999; Thorson, Jannot, & Somers, 2017), its integration within a size-structured spatiotemporal model remains a topic for future research. These three unmodelled mechanisms (additional environmental variables, species interactions and cohort-specific distribution) will all be at least as difficult to forecast as global water temperature. Therefore, identifying mechanisms for historical variation in COG may not translate to improved forecasts of future variation. However, we still argue that disentangling the multiple drivers of historical COG is a necessary first step to forecasting future distribution shifts.

We also acknowledge several important caveats regarding our approach to identify temperature impacts on pollock distribution shifts in the EBS. Most importantly, we have not included lagged effects of local or regional temperatures (either within or among years), and recent research has highlighted the potentially important effect of lagged environmental conditions on explaining local density (Blonder et al., 2017). If bottom temperature varies among months within a given year, for example, then different months within a year may have weaker or stronger correlation with a given biological variable (e.g., Black, 2009). Best practices for including lagged effects is also an ongoing research topic when estimating environmental impacts on recruitment for marine fishes (Szuwalski, Vert-Pre, Punt, Branch, & Hilborn, 2015), and future studies of pollock distribution shift could use exploratory methods to identify important lags for environmental variables. We also acknowledge that the impact of temperature on local density may be highly nonlinear. We have included a quadratic impact of local bottom temperature and a linear impact of regional cold pool size, and approximating temperature impacts in this way may have decreased the variance explained by temperature relative to using a highly nonlinear model for temperature impacts. Finally, we note that including additional missing variables may increase the explanatory power of temperature. For a hypothetical example, temperature impacts may have varied before and after the 1998 regime shift (Rodionov & Overland, 2005), so including the interactions of temperature and a dummy variable (representing before/after the regime

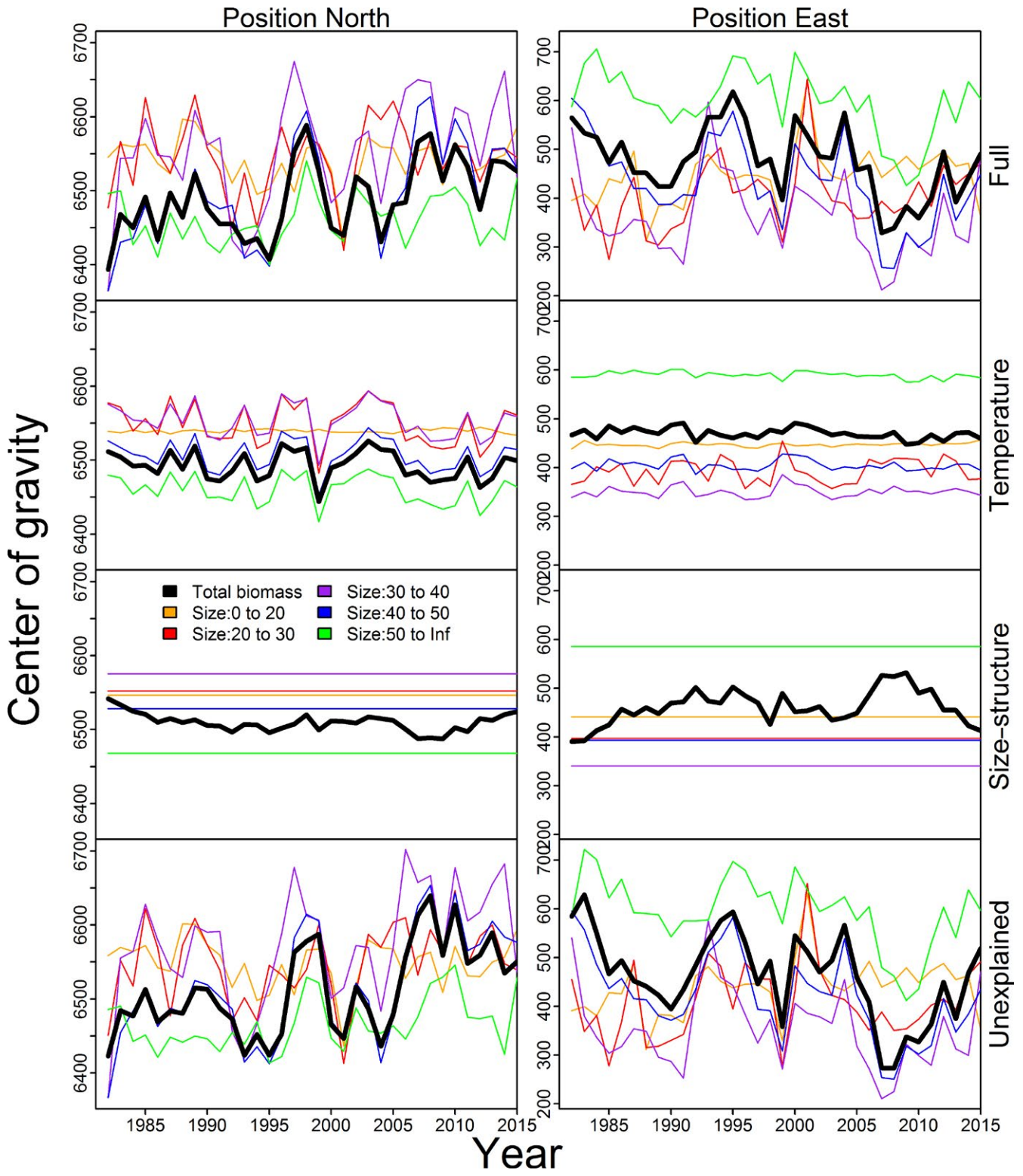

FIGURE 4 Time-series predictions of centre of gravity (COG, northward: left column; eastward: right column) given the fitted model (1st row), only temperature effects (2nd row), only recruitment variation effects (3rd row) or only unexplained variation (4th row), where the COG for total biomass (black) is compared with COG for each individual size-category (orange: 1-year-olds; red: 2-year-olds; purple: intermediate sizes; blue: adults; green: largest individuals)

shift) could increase the estimated importance of temperature. Future research could also use simulation testing to explore our ability to detect temperature signals of varying magnitude. We therefore interpret out results as a starting point for ongoing statistical and exploratory research seeking to attribute population-wide distribution shifts for pollock to factors affecting local density.

Finally, we provide software to implement the vector-autoregressive spatiotemporal model as an R package called "VAST". This software can also be used to estimate size-specific indices of biomass, for use as an input into size-structured stock assessment models (Punt, Huang, & Maunder, 2013), or to jointly model the spatial distribution for multiple species simultaneously (Ovaskainen, Roy, Fox, & Anderson, 2016; Thorson, Scheuerell, et al., 2015). We encourage broader use of size-structured spatiotemporal models to answer whether temperature generally explains a small or large portion of historical distribution shifts for a wide variety of marine fishes.

ACKNOWLEDGEMENTS

We thank Bob Lauth for data regarding the cold pool size in each year (shown in Figure 1) and Kirstin Holsman for discussions regarding the distribution of pollock. We also thank Aaron Berger, Paul Spencer, Jim Hastie, and Michelle McClure and two anonymous reviewers for comments on an earlier draft.

REFERENCES

Alverson, D. L., & Pereyra, W. T. (1969). Demersal fish explorations in the northeastern Pacific Ocean – an evaluation of exploratory fishing methods and analytical approaches to stock size and yield forecasts. *Journal of the Fisheries Research Board of Canada*, *26*, 1985–2001.

Bailey, K. M. (1989). Interaction between the vertical distribution of juvenile walleye pollock *Theragra chalcogramma* in the eastern Bering Sea, and cannibalism. *Marine Ecology Progress Series*, *53*, 205–213.

Bez, N. (2002). Global fish abundance estimation from regular sampling: The geostatistical transitive method. *Canadian Journal of Fisheries and Aquatic Sciences*, *59*, 1921–1931.

Black, B. A. (2009). Climate-driven synchrony across tree, bivalve, and rockfish growth-increment chronologies of the northeast Pacific. *Marine Ecology Progress Series*, *378*, 37–46.

Blonder, B., Moulton, D. E., Blois, J., Enquist, B. J., Graae, B. J., Macias-Fauria, M., … Svenning, J.-C. (2017). Predictability in community dynamics. *Ecology Letters*, *20*, 293–306.

Cheung, W. W. L., Lam, V. W. Y., Sarmiento, J. L., Kearney, K., Watson, R., & Pauly, D. (2009). Projecting global marine biodiversity impacts under climate change scenarios. *Fish and Fisheries*, *10*, 235–251.

Ciannelli, L., Fauchald, P., Chan, K. S., Agostini, V. N., & Dingsør, G. E. (2008). Spatial fisheries ecology: Recent progress and future prospects. *Journal of Marine Systems*, *71*, 223–236.

Dorn, M. W. (1995). The effects of age composition and oceanographic conditions on the annual migration of Pacific whiting, *Merluccius productus*. *California Cooperative Oceanic Fisheries Investigations Report* (pp. 97–105).

Ernst, B., Orensanz, J. M., & Armstrong, D. A. (2005). Spatial dynamics of female snow crab (*Chionoecetes opilio*) in the eastern Bering Sea. *Canadian Journal of Fisheries and Aquatic Sciences*, *62*, 250–268.

Fissel, B., Dalton, M., Felthoven, R., Garber-Yonts, B., Haynie, A., Himes-Cornell, A., … Seung, C. (2015). *Stock assessment and fishery evaluation report for the groundfish fisheries of the Gulf of Alaska and Bering Sea/Aleutian Islands area: Economic status of the groundfish fisheries off Alaska, 2014*. Seattle, WA: NPFMC Economic SAFE.

Garrison, L. P., Link, J. S., Kilduff, D. P., Cieri, M. D., Muffley, B., Vaughan, D. S., … Latour, R. J. (2010). An expansion of the MSVPA approach for quantifying predator–prey interactions in exploited fish communities. *ICES Journal of Marine Science: Journal du Conseil*, *67*, 856.

Gratwicke, B., Petrovic, C., & Speight, M. R. (2006). Fish distribution and ontogenetic habitat preferences in non-estuarine lagoons and adjacent reefs. *Environmental Biology of Fishes*, *76*, 191–210.

Hicks, A. C., Taylor, N., Grandin, C., Taylor, I. G., & Cox, S. (2014). *Status of the Pacific hake (whiting) stock in U.S. and Canadian waters in 2013*. Seattle, WA: International Joint Technical Committee for Pacific Hake.

Ianelli, J. N., Honkalehto, T., Barbeaux, S., & Kotwicki, S. (2015). *Assessment of the walleye pollock stock in the Eastern Bering Sea* (pp. 53–152). Seattle, WA: Alaska Fisheries Science Center.

Kotwicki, S., Buckley, T. W., Honkalehto, T., & Walters, G. (2005). Variation in the distribution of walleye pollock (*Theragra chalcogramma*) with temperature and implications for seasonal migration. *Fishery Bulletin*, *103*, 574–587.

Kotwicki, S., De Robertis, A., von Szalay, P., & Towler, R. (2009). The effect of light intensity on the availability of walleye pollock (*Theragra chalcogramma*) to bottom trawl and acoustic surveys. *Canadian Journal of Fisheries and Aquatic Sciences*, *66*, 983–994.

Kotwicki, S., Ianelli, J. N., & Punt, A. E. (2014). Correcting density-dependent effects in abundance estimates from bottom-trawl surveys. *ICES Journal of Marine Science: Journal du Conseil*, *71*, 1107–1116.

Kotwicki, S., & Lauth, R. R. (2013). Detecting temporal trends and environmentally-driven changes in the spatial distribution of bottom fishes and crabs on the eastern Bering Sea shelf. *Deep Sea Research Part II: Topical Studies in Oceanography*, *94*, 231–243.

Kristensen, K., Nielsen, A., Berg, C. W., Skaug, H., & Bell, B. M. (2016). TMB: Automatic differentiation and laplace approximation. *Journal of Statistical Software*, *70*, 1–21.

Kristensen, K., Thygesen, U. H., Andersen, K. H., & Beyer, J. E. (2014). Estimating spatio-temporal dynamics of size-structured populations. *Canadian Journal of Fisheries and Aquatic Sciences*, *71*, 326–336.

Lindgren, F., Rue, H., & Lindström, J. (2011). An explicit link between Gaussian fields and Gaussian Markov random fields: The stochastic partial differential equation approach. *Journal of the Royal Statistical Society: Series B (Statistical Methodology)*, *73*, 423–498.

Maunder, M. N., & Punt, A. E. (2004). Standardizing catch and effort data: A review of recent approaches. *Fisheries Research*, *70*, 141–159.

Nichol, D. G. (1998). Annual and between-sex variability of yellowfin sole, *Pleuronectes asper*, spring-summer distributions in the eastern Bering Sea. *Fishery Bulletin*, *96*, 547–561.

Nøttestad, L., Giske, J., Holst, J. C., & Huse, G. (1999). A length-based hypothesis for feeding migrations in pelagic fish. *Canadian Journal of Fisheries and Aquatic Sciences*, *56*, 26–34.

Ovaskainen, O., Roy, D. B., Fox, R., & Anderson, B. J. (2016). Uncovering hidden spatial structure in species communities with spatially explicit joint species distribution models. *Methods in Ecology and Evolution*, *7*, 428–436.

Perry, A. L., Low, P. J., Ellis, J. R., & Reynolds, J. D. (2005). Climate change and distribution shifts in marine fishes. *Science*, *308*, 1912–1915.

Petitgas, P. (2001). Geostatistics in fisheries survey design and stock assessment: Models, variances and applications. *Fish and Fisheries*, *2*, 231–249.

Pinsky, M. L., Worm, B., Fogarty, M. J., Sarmiento, J. L., & Levin, S. A. (2013). Marine taxa track local climate velocities. *Science*, *341*, 1239–1242.

Punt, A. E., Huang, T., & Maunder, M. N. (2013). Review of integrated size-structured models for stock assessment of hard-to-age crustacean and mollusc species. *ICES Journal of Marine Science: Journal du Conseil*, *70*, 16–33.

R Core Team (2015). *R: A language and environment for statistical computing*. Vienna, Austria: R Foundation for Statistical Computing.

Rodionov, S., & Overland, J. E. (2005). Application of a sequential regime shift detection method to the Bering Sea ecosystem. *ICES Journal of Marine Science*, *62*, 328–332.

Shelton, A. O., Thorson, J. T., Ward, E. J., & Feist, B. E. (2014). Spatial semiparametric models improve estimates of species abundance and distribution. *Canadian Journal of Fisheries and Aquatic Sciences*, *71*, 1655–1666.

Sibert, J. R., Hampton, J., Fournier, D. A., & Bills, P. J. (1999). An advection–diffusion–reaction model for the estimation of fish movement parameters from tagging data, with application to skipjack tuna (*Katsuwonus pelamis*). *Canadian Journal of Fisheries and Aquatic Sciences*, *56*, 925–938.

Silver, N. (2015). *The signal and the noise: Why so many predictions fail–but some don't*. New York, NY: Penguin Books.

Skaug, H., & Fournier, D. (2006). Automatic approximation of the marginal likelihood in non-Gaussian hierarchical models. *Computational Statistics & Data Analysis*, *51*, 699–709.

Somerton, D. A., & Weinberg, K. L. (2001). The affect of speed through the water on footrope contact of a survey trawl. *Fisheries Research*, *53*, 17–24.

Spencer, P. D. (2008). Density-independent and density-dependent factors affecting temporal changes in spatial distributions of eastern Bering Sea flatfish. *Fisheries Oceanography*, *17*, 396–410.

Spencer, P. D., Holsman, K. K., Zador, S., Bond, N. A., Mueter, F. J., Hollowed, A. B., & Ianelli, J. N. (2016). Modelling spatially dependent predation mortality of eastern Bering Sea walleye pollock, and its implications for stock dynamics under future climate scenarios. *ICES Journal of Marine Science: Journal du Conseil*, *73*, 1330–1342.

Stabeno, P. J., Bond, N. A., Kachel, N. B., Salo, S. A., & Schumacher, J. D. (2001). On the temporal variability of the physical environment over the south-eastern Bering Sea. *Fisheries Oceanography*, *10*, 81–98.

Stauffer, G. (2004). *NOAA protocols for groundfish bottom trawl surveys of the nation's fishery resources. NOAA Tech. Memo. NMFS-F/SPO-65*.

Szuwalski, C. S., Vert-Pre, K. A., Punt, A. E., Branch, T. A., & Hilborn, R. (2015). Examining common assumptions about recruitment: A meta-analysis of recruitment dynamics for worldwide marine fisheries. *Fish and Fisheries*, *16*, 633–648.

Thorson, J. T., & Barnett, L. A. K. (2017). Comparing estimates of abundance trends and distribution shifts using single- and multispecies models of fishes and biogenic habitat. *ICES Journal of Marine Science: Journal du Conseil*. Retrieved from: https://academic.oup.com/icesjms/article-abstract/doi/10.1093/icesjms/fsw193/2907795/Comparing-estimates-of-abundance-trends-and?redirectedFrom=PDF. doi: 10.1093/icesjms/fsw193.

Thorson, J. T., Ianelli, J. N., Larsen, E. A., Ries, L., Scheuerell, M. D., Szuwalski, C., & Zipkin, E. F. (2016). Joint dynamic species distribution models: A tool for community ordination and spatio-temporal monitoring. *Global Ecology and Biogeography*, *25*, 1144–1158.

Thorson, J. T., Ianelli, J. N., Munch, S. B., Ono, K., & Spencer, P. D. (2015). Spatial delay-difference models for estimating spatiotemporal variation in juvenile production and population abundance. *Canadian Journal of Fisheries and Aquatic Sciences*, *72*, 1897–1915.

Thorson, J. T., Jannot, J., & Somers, K. (2017). Using spatio-temporal models of population growth and movement to monitor overlap between human impacts and fish populations. *Journal of Applied Ecology*, *54*, 577–587.

Thorson, J. T., Munch, S., & Swain, D. (2017). Estimating partial regulation in spatio-temporal models of community dynamics. *Ecology*, *98*, 1277–1289.

Thorson, J. T., Pinsky, M. L., & Ward, E. J. (2016). Model-based inference for estimating shifts in species distribution, area occupied and centre of gravity. *Methods in Ecology and Evolution*, *7*, 990–1002.

Thorson, J. T., Scheuerell, M. D., Shelton, A. O., See, K. E., Skaug, H. J., & Kristensen, K. (2015). Spatial factor analysis: A new tool for estimating joint species distributions and correlations in species range. *Methods in Ecology and Evolution*, *6*, 627–637.

Thorson, J. T., Shelton, A. O., Ward, E. J., & Skaug, H. J. (2015). Geostatistical delta-generalized linear mixed models improve precision for estimated abundance indices for West Coast groundfishes. *ICES Journal of Marine Science: Journal du Conseil*, *72*, 1297–1310.

Warton, D. I., Blanchet, F. G., O'Hara, R. B., Ovaskainen, O., Taskinen, S., Walker, S. C., & Hui, F. K. (2015). So many variables: Joint modeling in community ecology. *Trends in Ecology & Evolution*, *30*, 766–779.

Weinberg, K. L., & Kotwicki, S. (2008). Factors influencing net width and sea floor contact of a survey bottom trawl. *Fisheries Research*, *93*, 265–279.

Wyllie-Echeverria, T., & Wooster, W. S. (1998). Year-to-year variations in Bering Sea ice cover and some consequences for fish distributions. *Fisheries Oceanography*, *7*, 159–170.

SUPPORTING INFORMATION

Additional Supporting Information may be found online in the supporting information tab for this article.

How to cite this article: Thorson JT, Ianelli JN, Kotwicki S. The relative influence of temperature and size-structure on fish distribution shifts: A case-study on Walleye pollock in the Bering Sea. *Fish Fish*. 2017;18:1073–1084. https://doi.org/10.1111/faf.12225